Research Article | Vol. 29, No. 2 / 18 January 2021 / Optics Express 1532
Optics EXPRESS

Accurate non-linear calculation model for decoupling thermal and mechanical loading effects in the OBR measurements

SHAOQUAN WANG* AND KASPAR LASN

Department of Mechanical and Industrial Engineering (MTP), Norwegian University of Science and Technology (NTNU), Richard Birkelands vei 2B, 7491, Trondheim, Norway
*shaoquan.wang@ntnu.no

Abstract: Fiber optic sensors are increasingly used in several fast-growing industries. Aerospace, energy storage, and the medical sector consider new implementations of optical fibers mainly for condition monitoring purposes. Applications using optical fibers entail measurements of distributed strains and temperatures. However, the spectral shifts of transmitted and reflected light are simultaneously sensitive to both of these influences. This coupled sensitivity can introduce large errors for signal interpretation. An accurate calculation model for signal decoupling is necessary to distinguish pure mechanical strains from pure thermal loading. Approaches where the spectral shift is assumed to vary linearly with temperature give large errors when the temperature variation is high. This investigation derives and validates a new temperature formula that is used for high precision strain and temperature discrimination. The non-linear temperature formula is deduced from physics-based models and is validated with Rayleigh backscattering based OBR measurements. Our calculation approach demonstrates improved accuracy over an extended temperature range. The relationship between strain and temperature effects in the coupled mechanical and thermal loading environment is further studied in detail.

1. Introduction

More than 60 different optical fiber sensor types have been developed as future sensors in previous decades [1,2]. Compared to conventional electrical sensors, optical fibers have several distinguishing advantages: (i) immunity to electromagnetic interference and environmental corrosion; (ii) small size and insignificant disturbance for the integrity of the structure; (iii) high temperature resistance; (iv) a lifetime exceeding 25 years [3–5]. In addition, optical fibers can multiplex a large number of sensors along a single fiber and set up a distributed optical fiber sensors (DOFS) network. By measuring the intrinsic backscattering variation in the fiber caused by external perturbations, the DOFS techniques based on multi fiber Bragg grating (FBG), Raman, Brillouin, and Rayleigh backscattering have been developed successfully. Nowadays, the DOFS are used for structural health monitoring in industrial infrastructure, in aerospace components, in architectural structures, and in human health applications.

Today, one of the most significant limitations for using the DOFS is their coupled sensitivity to both temperature and strain. For instance, temperature variations along the sensing fiber will introduce errors for the strain measurement. The ability to distinguish between strain and temperature effects is critical for the large-scale success of DOFS applications. Rayleigh backscattering spectrum has been adopted in DOFS to determine strain and temperature along the entire length of an optical fiber. Modeled as a weak FBG with a random period, changes in the refractive index or in the physical optical fiber length cause the Rayleigh backscattering spectral (RBS) shift in frequency. The RBS shift shows a cross-sensitivity to both strain and temperature similar to FBGs. In the field of DOFS techniques based on FBGs, different approaches have been proposed to discriminate strain and temperature [6–9]. These methods utilize well-designed

#410686 https://doi.org/10.1364/OE.410686
Journal © 2021 Received 21 Sep 2020; revised 12 Nov 2020; accepted 24 Nov 2020; published 11 Jan 2021

Optics EXPRESS

optical fiber sensor systems which have different temperature and strain sensitivities. Once the temperature and strain coefficients of the optical fiber are known, the temperature and strain variation can be determined by using the inverse of the coefficients' matrix. Most recent strain/temperature discrimination methods in Rayleigh backscattering based DOFS are analogous to the decoupling techniques of FBGs [10–14]. One solution utilizes the specral shifts of the fast and slow modes of birefringence by autocorrelation and by cross-correlation of RBS shifts in the polarization maintaining fiber (PMF) [10,11]. The distributed autocorrelations of the Rayleigh spectral signature are strongly related to thermal effects on the fiber, while distributed cross-correlations of the Rayleigh spectral signature are related to both thermal and strain effects. Another method uses stimulated Brillouin scattering and Rayleigh backscattering in a single-mode fiber (SMF) to discriminate between the temperature and strain changes [12,13]. The Brillouin frequency shift and the distributed RBS shift were induced by strain and temperature variations. Although both methods are sensitive to temperature and strain, their sensitivities are different and independent from each other; therefore, a complete temperature and strain discrimination can be realized by measuring a pair of spectral shifts along the PMF sensor. Although the methods above conveniently utilize a single fiber for dual-measurements of strain and temperature, they are also complicated and costly. Measuring Brillouin scattering and Rayleigh backscattering in a PMF requires two systems of measurement techniques. PMF is also more expensive compared to single-mode optical fibers for large applications. A simple way to achieve discrimination utilizes a SMF and a reduced-cladding SMF [14], because the temperature and strain coefficients of the two optical fibers are different. However, two types of SMFs must be attached closely side by side, and two interferometers are needed for measurements when using this system.

All previous strain/temperature discrimination methods for DOFS based on Rayleigh backscattering (developing from the techniques of FBGs) assume that strain- and thermally-induced effects are both linear with respect to RBS shifts. The superposition of strain and temperature induced spectral changes has also been found to apply well for FGBs. Rayleigh scattering-based DOFS have been successfully used to perform temperature measurements under thermal conditions [15,16], and coupled with irradiation [17], or humidity [18]. In these investigations, RBS shifts are modeled using linear relations to temperature with good accuracy within temperature ranges from ca. 0 °C to ca. 75 °C. However, obvious measurement errors occur for linear fitting at high temperatures (> 80 °C) and at cryogenic low temperatures (< -73 °C). Additionally, the temperature induced RBS shifts are shown to be humidity and low dose radiation independent. The review of existing literature for Rayleigh scattering-based DOFS shows clearly that superposition/decoupling of strain and temperature induced spectral changes has not been addressed with sufficient rigor thus far, especially for thermal conditions beyond typical inside and outside temperatures.

In this paper, a simple and effective calculation model is realized for strain and temperature discrimination by using the OBR, a high resolution DOFS technology based on Rayleigh backscattering. Identical physically separated optical fibers are used to compensate for temperature effects. During the procedure, the measurement fiber experiences a coupled mechanical and thermal loading while the compensation fiber only the thermal loading. The temperature effect for the OBR is shown to be nonlinear due to the thermo-optic coefficient and its relationship with temperature. Improving state of the art, a polynomial temperature calculation formula is deduced from a physics-based model. High precision temperature measurements over an extended temperature range are carried out by using a customized test set-up where OBR measurements are taken inside the temperature chamber of a DMTA (dynamic mechanical thermal analysis) test instrument. The relationship between strain and temperature effects is studied in the coupled mechanical and thermal loading environment. A novel high-precision calculation model is applied to subtract temperature effects from the coupled measurement data.

Optics EXPRESS

2. Experimental setup

2.1. Interrogator devices and sensors

As shown in Fig. 1(a), a reflectometer OBR 4600 from Luna Instruments is used as the interrogator device for the DOFS measurements. The optical fiber SMB-E1550H from OFS Fitel with a silica/silica/polyimide structure and a core diameter 6.5 µm, a cladding diameter 125 µm, and a coating of 155 µm diameter is used for sensing strain and temperature. The independent temperature measuring system in the experiment consists of an electronic temperature sensor with accompanying data acquisition equipment. The temperature sensor is a special K-type wire thermocouple SRTC-TT-KI-40-1M and the data is read and stored by a DP9800-TC digital thermometer from OMEGA Engineering.

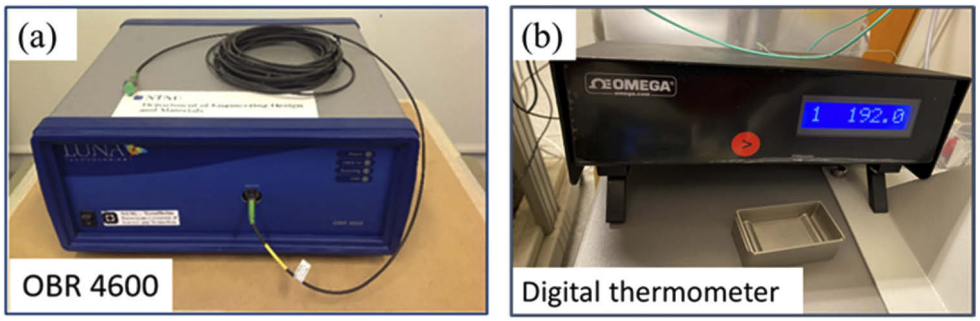

Fig. 1. (a) Interrogator apparatus LUNA OBR 4600, (b) Thermometer DP9800-TC.

2.2. Mechanical and thermal loading set-up

A customized experimental set-up is used to investigate the combined loading effect from strain and temperature on the OBR RBS shift measurements. The set-up assembly (Fig. 2) consists of a temperature chamber, a clamper, a perforated tube, and a dead weight system. The temperature chamber from a NETZSCH Eplexor DMTA machine is used to control the temperature around the optical fibers. The chamber has capacity from -150 °C to 500 °C. However, a smaller range from -130 °C to 240 °C is used for this investigation. The clamper is attached to the ceiling of the chamber to fix the top of the optical fiber. The optical fiber then passes through a perforated tube which protects it from vibrations induced by the cooling fan. The mechanical loading on the fibers is created by a system of dead weights. One thermocouple is plugged into the perforated tube to provide accurate and independent temperature information about the optical fiber measurement region. By these small modifications to the DMTA temperature chamber, a controlled thermal and mechanical loading can be applied to individual fibers, or groups of optical fibers simultaneously.

2.3. Measurement procedure

Before each OBR measurement, the DMTA chamber temperature is maintained for two minutes to fully heat or cool down the optical fiber sensor and the measurement system around it. During the testing procedure the optical fibers are heated from room temperature to the highest temperature first and then cooled down to the lowest temperature of the range. The signals from the optical fibers and the K-type sensors are recorded simultaneously over ca. 5 seconds period at each temperature measurement. The average RBS shift over the measurement zone of the optical fiber is recorded, while the mean temperature of the K-type sensor is used as an independent temperature measurement. The K-type sensor data is used for the temperature values on the

Optics EXPRESS

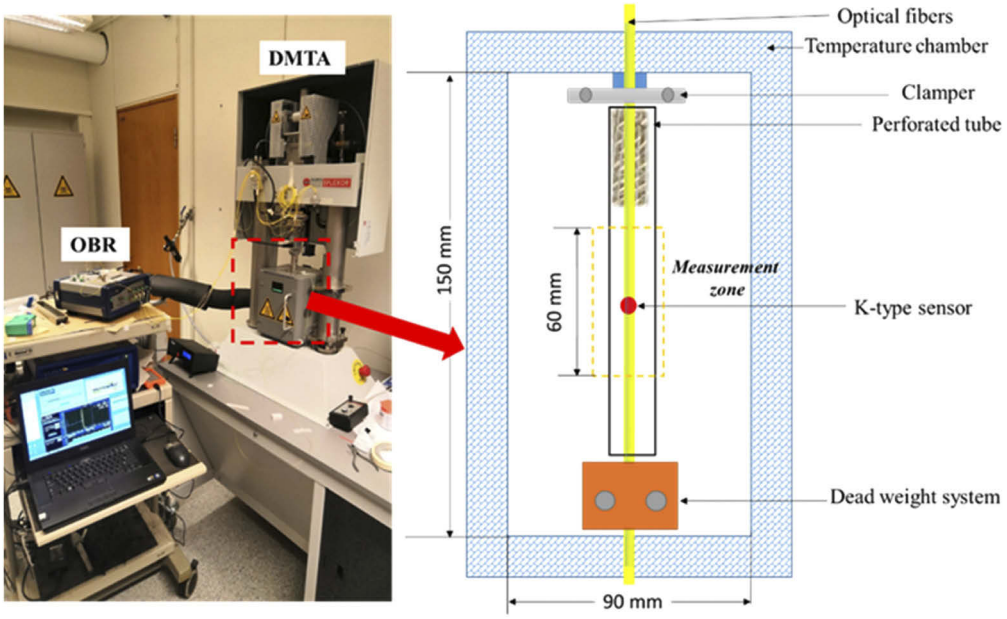

Fig. 2. Mechanical and thermal loading instrument with the OBR system.

x-axes of figures shown in the following Sections. The instrumentation parameters for OBR 4600 and DP9800-TC digital thermometer are shown in Table 1.

Table 1. Equipment parameters.

OBR 4600					
Incident light	Sensor diameter	Scan mode	Sensing range	Gauge length	Sensor spacing
$\bar{\lambda} = 1550$ nm	155 μm	Single scan-standard	60 mm	10 mm	4 mm
Digital thermometer					
Sensor type		Sensor diameter	Limits of error		
K-type (SRTC-TT-KI-40-1M)		190 μm	0.75% above 0 °C and 2.0% below 0 °C		

3. Results and discussion

3.1. Thermal loading effects

In this Section, a polynomial formula is first deduced from the underlying physics. Thereafter it is applied for precise temperature measurements with the OBR. The non-linear formula is compared to the usual linear formula under pure thermal loading conditions over four temperature ranges. It has to be pointed out that FBGs are outside of the experimental scope of current investigation. However, the analyses approach described below is also applicable to these optical fiber sensors.

3.1.1. Polynomial temperature formula

As described by Wang [19], the distributed Rayleigh backscattering along the length of the optical fiber can be modeled as a weak FBG with a random period. Thus the RBS shifts induced by the temperature change are identical to FBGs, expressed by [20]:

Optics EXPRESS

$$\frac{\Delta v(T)}{\bar{v}} = -\frac{\Delta\lambda(T)}{\bar{\lambda}} = -\left(\frac{1}{\Lambda}\Delta\Lambda(T) + \frac{1}{n}\Delta n(T)\right) \tag{1}$$

where $\bar{v}$ and $\bar{\lambda}$ are the mean optical frequency and the mean wavelength of the scan, $\Delta v(T)$ is the measured spectral shift of the light, n is the effective refractive index and Λ is the grating period. The temperature sensitivity of the spectrum arises from the thermal expansion, and the refractive index change of the glass fiber. The first term on the right-hand side corresponds to the coefficient of thermal expansion (CTE) of silica (α), and the second term corresponds to the thermo-optic coefficient of the fiber (β). Thus, Eq. (1) transforms into [21]:

$$\frac{\Delta v(T)}{\bar{v}} = -\left(\int \alpha(T)dT + \int \beta(T)dT\right) = -\int K_T(T)dT \tag{2}$$

where the temperature conversion factor is defined as $K_T\ (T) = \alpha+\beta$. Thus, the temperature induced RBS shift Δv_T between the OBR reference scan (fiber temperature $T = T_r$) and the OBR measurement scan (fiber temperature $T = T_m$) in the Rayleigh scattering-based DOFS is calculated by Eq. (3), where c is the speed of light and $\bar{\lambda}$ is the center wavelength of the scan (1550 nm for the current device):

$$\Delta v_T = -\frac{c}{\bar{\lambda}} \cdot \int_{T_r}^{T_m} K_T(T)dT \tag{3}$$

In the single mode silica optical fiber, the value of α is approximately $0.55 \cdot 10^{-6}$/°C, while the value of β is from 10^{-8} to $8.5 \cdot 10^{-6}$/°C [22]. Simplifying the values of α and β as constants, coefficient K_T becomes equal to $6.45 \cdot 10^{-6}$/°C for the germanosilicate core fiber used in this research. The relationship between the temperature change $\Delta T = T_m$ - T_r and the temperature change induced RBS shift Δv_T for this OBR measurement set-up is sometimes described in even simpler form, using C_T as the constant equal to -1.248 GHz/°C, in:

$$\Delta v_T = C_T \cdot \Delta T \tag{4}$$

However, in the infrared wavelength region adopted by the OBR system, the β of silica glass has also been found to be strongly dependent of temperature [23–26]. The relationship between temperature and refractive index n exhibits a non-linear behavior at high temperatures [16]. The optical properties of materials (including refractive index n) are determined by coupling various types of oscillators to the electromagnetic radiation field. Corte et al. [24] uses a single oscillator model to obtain the refractive index n of silica by:

$$n^2 = 1 + \frac{E_p^2}{E_g^2 - E^2} \tag{5}$$

where E_p is electronic plasma energy, E the photon energy, and E_g is the optical band gap average energy. The E_p is inversely proportional to the volume, and the E_g is dependent on the temperature. In order to show the temperature dependence of the refractive index, a physically meaningful model from Gorachand Ghosh [25,26] is hereby applied. In this model, $E_{ig}^2 = E_g E_{eg}$, where E_{eg} is the excitonic band gap and E_{ig} is the isentropic band gap in the infrared region as shown in the energy level diagram (Fig. 3). As shown in Eq. (6), the model of Ghosh [25] includes the first right-hand term which is related to the CTE (α), and the second right-hand term related to optical band gap temperature coefficients E_{eg} and E_{ig}. The isentropic band gap E_{ig} is considered invariant with temperature, thus the temperature shift of excitonic band gap E_{eg}

Optics EXPRESS

controls the quantitive behavior of *dn/dT* [25]. A simple model for β is now expressed by Eq. (7).

$$\beta = \frac{dn}{dt} = \frac{n^2-1}{2n}(-3\alpha) - \frac{n^2-1}{2n}\left(\frac{1}{E_{eg}} \cdot \frac{dE_{eg}}{dT} \cdot \frac{E_{ig}^2}{E_{ig}^2 - E^2}\right) \tag{6}$$

$$\beta = A(T) + B(T) \tag{7}$$

where thermo-optic coefficient β is controlled by two factors *A(T)* and *B(T)*. It is assumed that the first factor $A(T)$ represents the contribution from the CTE (α), and the second term, $B(T)$ represents the contribution of the excitonic band gap (E_{eg}). According to Ghosh [25], $A(T)$ has only a minor contribution to the temperature dependence of the refractive index compared to $B(T)$, and is viewed as constant a_0 in Eq. (8), while a quadratic function of temperature is used to express the contribution of *B(T)* as shown in Eq. (9) [25].

$$\beta = a_0 + B(T) \tag{8}$$

$$B(T) = b_0 + b_1 T + b_2 T^2 \tag{9}$$

Thereby, K_T also becomes expressed as a quadratic function of temperature:

$$K_T(T) = \alpha + \beta = \alpha + a_0 + B(T) = H_0 + H_1 T + H_2 T^2 \tag{10}$$

Finally, inserting Eq. (10) into Eq. (3), the latter can be rewritten and rearranged as:

$$\Delta\nu_T = -\frac{c}{\bar{\lambda}} \cdot \int_{T_r}^{T_m} K_T(T)dT = C_0(T_m - T_r) + C_1(T_m^2 - T_r^2) + C_2(T_m^3 - T_r^3) \tag{11}$$

where the temperature difference and the RBS shift between the reference test and the measurement test become related by the polynomial temperature formula. This formula is physics-based and enables high precision temperature measurements with the OBR. Based on analogy the formula is also applicable for the FBGs.

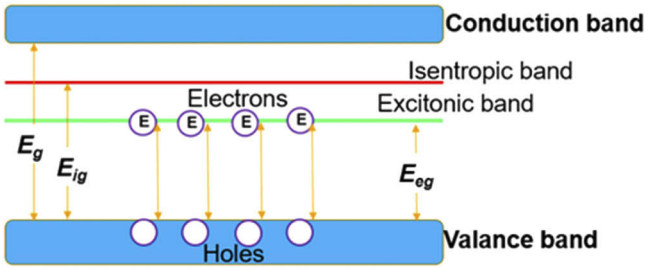

Fig. 3. Energy level diagram for silica glass.

3.1.2. Comparison between linear and polynomial formulas

A reference OBR test was implemented at $T_r = 30.6$ °C, and then a series of measurements were performed over a temperature range from –130 °C to 200 °C. Five independent optical fibers (A, B, C, D and E) were positioned simultaneously in the temperature chamber (see Fig. 2) without any mechanical loading. The measured RBS shift was fitted by the usual linear model and the new non-linear model separately to compare the difference between the two approaches. The measured data and the parameters of linear and non-linear curve fits are shown in Fig. 4 and in

Optics EXPRESS

Table 2, respectively. The linear model is described by $\Delta\nu_T = a + bT_m$, where $\Delta\nu_T$ is the RBS shift induced by thermal loading, T_m is the temperature of the measurement scan, $b = -\frac{c}{\lambda}K_T$, and a has the value of $\Delta\nu_T$ when $T_m = 0$ °C. The non-linear model is expressed by Eq. (11), where $T_r = 30.6$ °C (reference temperature). By using the linear curve fitting formula, the value of b = -1.225 GHz/°C was obtained, similar to $-\frac{c}{\lambda}K_T$ = -1.248 GHz/°C predicted previously in Section 3.1.1. The results in [15–18,27] show that linear fitting is reasonable within a small temperature range, however the discrepancies of using a linear formula become evident with temperatures far away from the reference temperature. The measurement data and the fitting curves of four different ranges symmetric to room temperature (see Fig. 4) are shown in Fig. 5 for visual comparison. In the smallest Range 1 (from -5 °C to 45 °C), both the linear and polynomial fitting curves agree with the measurement data, almost overlapping each other. With the expansion of the temperature range, the linear and polynomial fitting curves start to diverge from each other as shown for Range 2 (from -25 °C to 65 °C) and for Range 3 (from -85 °C to 125 °C). In the widest Range 4 (from -125 °C to 165 °C) only the non-linear curve is still acceptable for representing the measurement data.

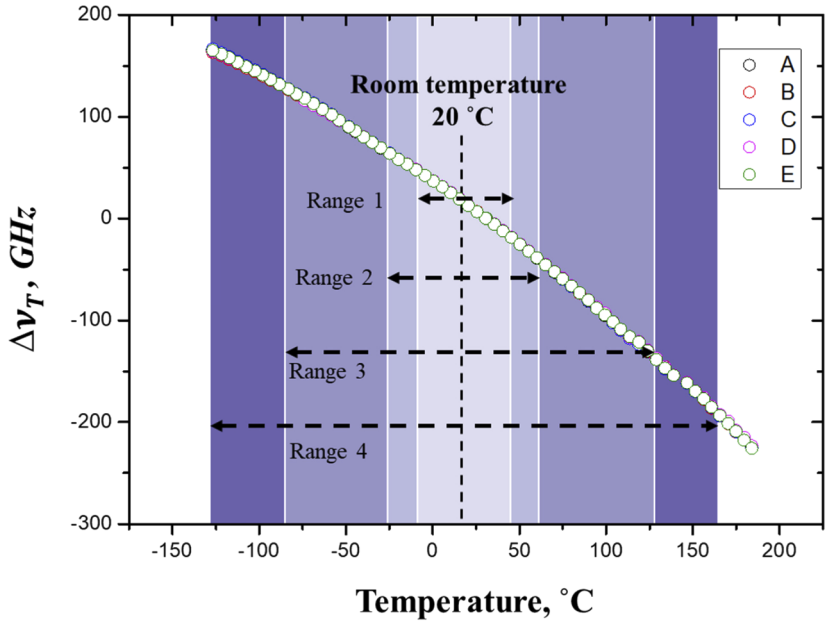

Fig. 4. Thermal loading induced RBS shifts measured by the OBR.

Table 2. Parameters obtained for linear and non-linear curve fitting models.

Linear fitting formula	$\Delta\nu_T = a + bT_m$
a (GHz)	37.76
b (GHz/°C)	-1.22
Polynomial fitting formula	$\Delta\nu_T = C_0(T_m - T_r) + C_1(T_m^2 - T_r^2) + C_2(T_m^3 - T_r^3)$
T_r (°C)	30.6
C_0 (GHz/°C)	1.18
C_1 (GHz/°C^2)	$1.35\cdot10^{-3}$
C_2 (GHz/°C^3)	$2.56\cdot10^{-7}$

Optics EXPRESS

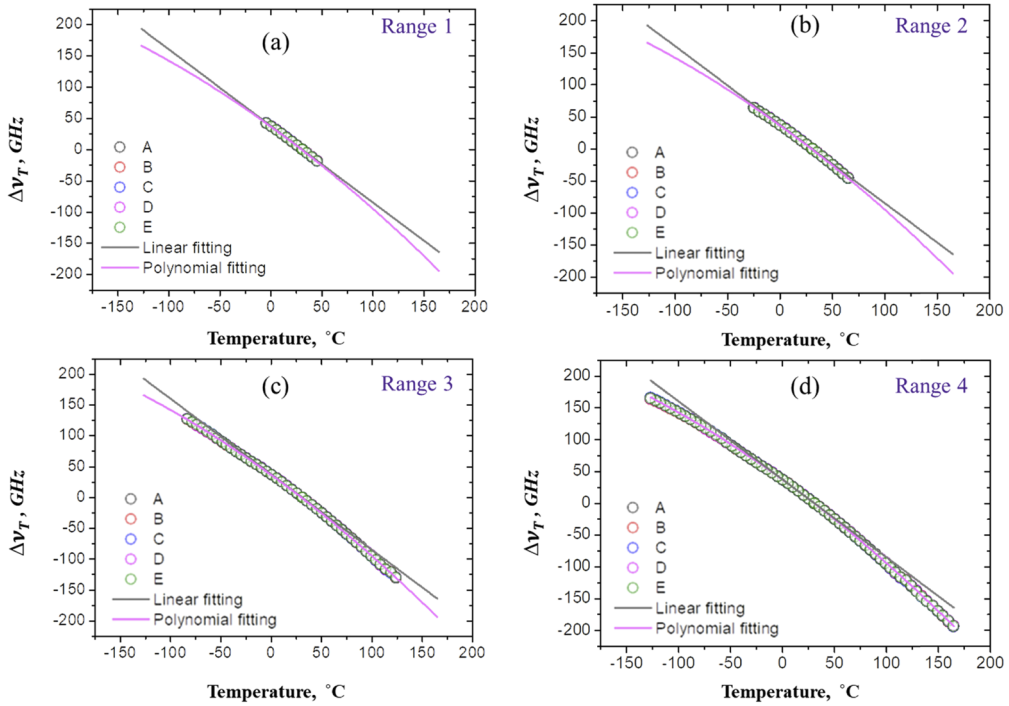

Fig. 5. The RBS shifts from the OBR and two alternative fitting curves when expanding the temperature range.

The adjusted R-squared metric is a modified version of the R-squared that is often used to evaluate the goodness-of-fit. High adjusted R-squared ≤1 indicates a good fit for the model. The adjusted R-squared is calculated for different temperature ranges and the results are shown in Fig. 6(a). The linear and non-linear fitting curves have very similar R^2 values for Range 1. When the temperature range becomes wider, as expected, the polynomial formula shows a greatly improved goodness-of-fit compared to the linear formula. Figure 6(b) dispalys the relative errors for the OBR temperature measurements (%error) when using the polynomial and the linear formulas:

$$\%error = \frac{|T_K - T_{OBR}|}{T_K} \cdot 100\% \tag{12}$$

where T_K is the temperature measured by the K-type thermocouple (Fig. 2) and T_{OBR} is the temperature measured by the OBR using the optical fiber. When the temperature remains within Range 1, there is little difference between the errors of polynomial and linear formulas (mostly < 5%). When the temperature exceeds Range 1, the polynomial formula shows a better temperature measurement precision over the whole measured temperature range. This experiment clearly demonstrates how the polynomial formula deduced from physics-based models improves the temperature measurement accuracy over an extended temperature range.

3.2. Mechanical loading effects

In the absence of temperature change, the mechanical strain relationship to the RBS shift can be written as [19]:

$$\varepsilon = -\frac{\bar{\lambda}}{c \cdot K_\varepsilon}\Delta\nu_M \tag{13}$$

Optics EXPRESS

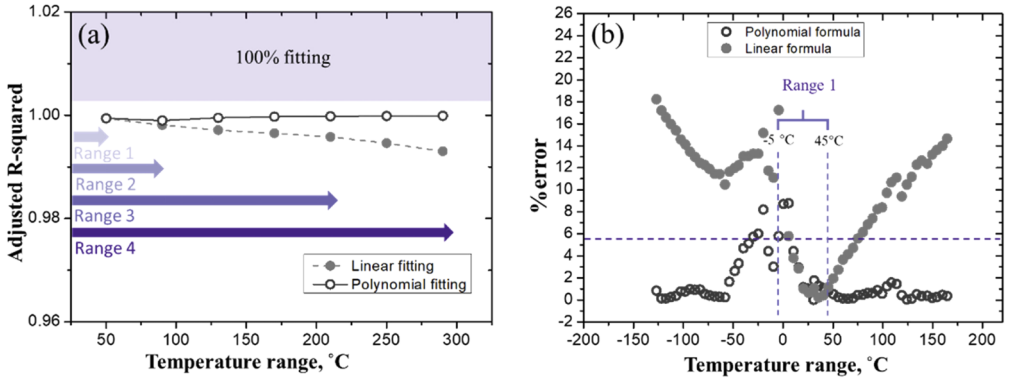

Fig. 6. The goodness of linear and polynomial fitting formulas with increasing temperature range: (a) Adjusted R-squared metric, (b) Relative error in the temperature measurement.

where K_ε is the strain coefficient and c is the speed of light. Previous research in our group has shown that K_ε is a constant with a value of 0.787 [28]. Thus, Eq. (13) yields the conversion factor: $\varepsilon = (-6.67\ \mu\varepsilon\ /\text{GHz})\ \Delta\nu_M$ for this OBR system.

3.3. Decoupling of mechanical and thermal loading effects

In this Section, the optical fibers are exposed to loading environments where a constant mechanical loading is coupled with varying thermal loads, and a constant thermal loading is coupled with varying mechanical loads. The relationship between strain and temperature effects for the RBS shift is experimentally investigated. Both, the linear and the non-linear (polynomial) formulas are applied for decoupling the mechanical and thermal loading effects. The relative errors of the two methods are compared.

3.3.1. Coupled mechanical and thermal loading

The optical fiber (OF1) was measured before and after it was loaded by a dead weight (60.23 g) at room temperature. This measurement gives the pure mechanical loading induced RBS shift ($\Delta\nu_{PM}$). The mean value of $\Delta\nu_{PM}$ over the measurement zone (Fig. 2) was calculated -95 GHz, shown by a green dashed line in Fig. 7(a). Subsequently, four additional independent optical fibers (OF2, OF3, OF4 and OF5) were placed into the temperature chamber. The measurement temperature of the chamber was varied from –125 °C to 240 °C. The RBS shift of OF1 ($\Delta\nu_{T\&M}$) was induced by coupled mechanical and thermal loading, while the other four fibers sensed only the same thermal loading without any mechanical loading. The $\Delta\nu_T$ is the average RBS shift of four optical fibers over their measurement zones. The $\Delta\nu_{T\&M}$ from OF1 shows the same nonlinear trend as $\Delta\nu_T$ but at values uniformly shifted below from $\Delta\nu_T$. The mechanical loading induced RBS shift $\Delta\nu_M$ (blue dotted line) is achieved by subtracting $\Delta\nu_T$ from $\Delta\nu_{T\&M}$. As evident from Fig. 7(a), the $\Delta\nu_M$ shows almost no variation with temperature and is in excellent agreement with $\Delta\nu_{PM}$.

Finally, another optical fiber (OF6) was subjected to a changing mechanical load by using different dead weights at 20.6 °C and at 30.1 °C separately. Figure 7(b) shows the $\Delta\nu_{T\&M}$ of OF6 at these two different temperatures while increasing the dead weight. The temperature difference induced $\Delta\nu_T$ is calculated by subtracting $\Delta\nu_{T\&M}$ at 20.6 °C from $\Delta\nu_{T\&M}$ at 30.1 °C at the same weight. Figure 7(b) shows that, at constant temperature, the mechanical loading affects the RBS shifts in the OBR linearly with applied dead weight (i.e., mechanical strain). The constant small difference between $\Delta\nu_{T\&M}$ (empty and solid circles) comes from the small temperature difference. The $\Delta\nu_T$ remains mechanical loading independent. These results show

Optics EXPRESS

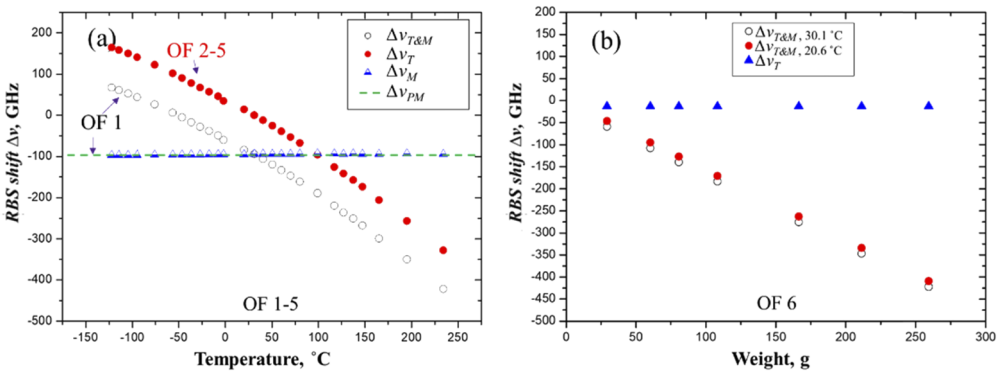

Fig. 7. The RBS shifts of optical fibers under coupled mechanical and thermal loading conditions, measured by the OBR.

that mechanical and thermally-induced effects can be considered independent from each other in the OBR measurements. Thus, the strain and the temperature effects can be added/subtracted by superposing the RBS shifts under coupled loading conditions.

3.3.2. Application of the polynomial formula

Mechanical loading is typically of main concern in the analysis of structures. That means the strain measurements are usually considered as the primary outputs from optical fiber sensors in engineering applications. The environmental temperatures can be obtained from separate thermal sensors and the influence of temperature is then subtracted from the overall loading effect. The linear and polynomial formulas are hereby applied to obtain pure mechanical strains from the coupled loading on the optical fiber. A new optical fiber (OF7) is loaded by using a dead weight of 29.32 g. The temperature data is obtained from an independent K-type thermal sensor. The pure $\Delta\nu_M$ is decoupled by the same subtraction of OBR measurements as seen in Fig. 7(a) and as described in Section 3.3.1. Figure 8 shows the $\Delta\nu_{T\&M}$ of OF7 while changing the surrounding temperature from –100 °C to 240 °C. The pure mechanical loading induced RBS shift $\Delta\nu_{RM}$ of OF7 was measured by the OBR at reference temperature (31.4 °C) before and after loading by the dead weight. The $\Delta\nu_{M-P}$ is the mechanical loading induced RBS shift when subtracting the $\Delta\nu_T$ calculated by the polynomial formula (Table 2) from $\Delta\nu_{T\&M}$, while the $\Delta\nu_{M-L}$ uses the linear formula (Table 2). As shown in Fig. 9(a), both the values of $\Delta\nu_{M-P}$ and $\Delta\nu_{M-L}$ are in very good agreement with the $\Delta\nu_{RM}$ from 0 °C to 50 °C. The difference between the $\Delta\nu_{M-P}$ and $\Delta\nu_{M-L}$ increases rapidly when the temperature is higher than 60 °C or lower than 0 °C.

The relative error (%*error*) between linear and polynomial formulas is also compared in Fig. 9(b):

$$\%error = \frac{|\Delta\nu_{RM} - \Delta\nu_M|}{\Delta\nu_{RM}} \cdot 100\% \tag{14}$$

where $\Delta\nu_M$ can be $\Delta\nu_{M-P}$ or $\Delta\nu_{M-L}$ based on the formula applied. When the temperature shift is small (e.g., as in Range 1 in Figs. 4–6), there is little practical difference between the measuring errors of the polynomial and the linear formulas (< 3%). When the temperatures exceed the range from ca. -25 °C to 75 °C, the linear model becomes poorly suited for decoupling mechanical and thermal loading effects in the OBR measurement. The polynomial model works well over the whole temperature range. Thus, the polynomial formula is a more accurate model to account for thermal loading effects. It enables to decouple RBS shifts with a higher precision over a wider range of temperatures.

Optics EXPRESS

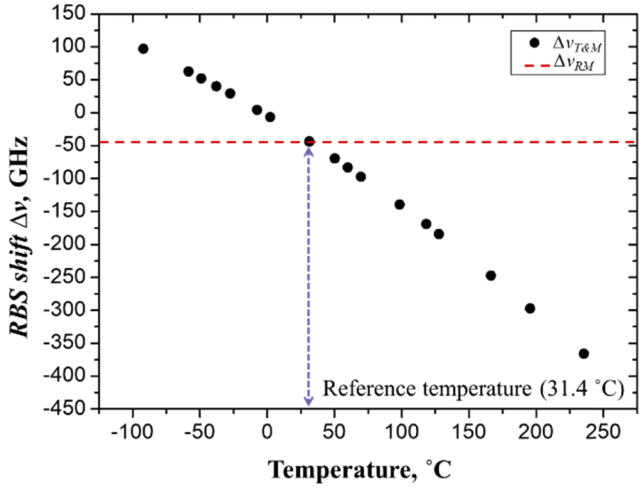

Fig. 8. The Δv_{RM} and the $\Delta v_{T\&M}$ of OF7 with a constant mechanical loading.

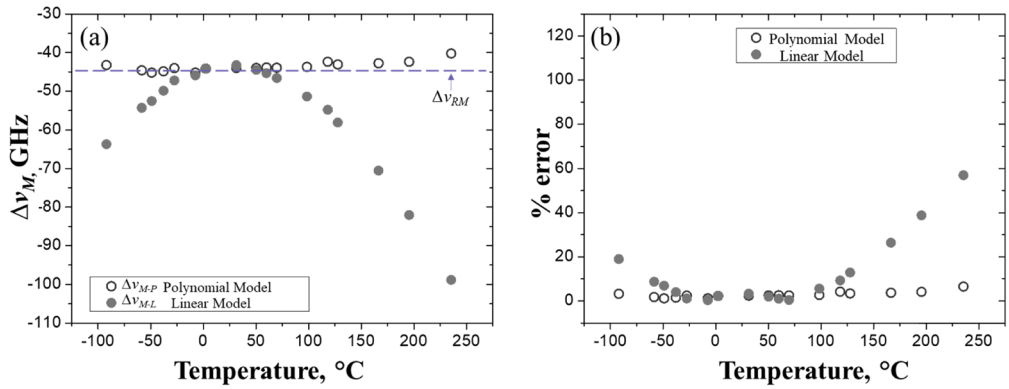

Fig. 9. A comparison between linear and polynomial models for an engineering application: (a) decoupled mechanical loading RBS shifts, (b) relative errors of RBS shift measurements.

4. Conclusions

1. Thermal loading induced RBS shifts of the OBR measurements are proven to be non-linear with temperature due to the relationship between the thermo-optic coefficient and temperature.

2. A polynomial formula is deduced from physics-based models for accurate temperature measurements with the OBR. The polynomial formula shows a higher temperature measurement precision than a linear formula over an extended temperature range.

3. Pure mechanical loading induced RBS shifts are shown to be linear with strain. Under coupled OBR measurement conditions, the mechanical and thermal loading effects are shown to be independent from each other. Pure mechanical strains can be obtained by subtracting the temperature effect (e.g. modelled by the polynomial formula) from the coupled RBS shift.

Optics EXPRESS

Funding

European Union's Horizon 2020 research and innovation programme and Hydrogen Europe and Hydrogen Europe Research (Grant ID: 826262).

Acknowledgments

This project has received funding from the Fuel Cells and Hydrogen 2 Joint Undertaking under grant agreement No. 826262, https://thor-fch2.eu/.

Disclosures

The authors declare no conflicts of interest.

References

1. L. Palmieri, "Distributed Optical Fiber Sensing Based on Rayleigh Scattering," The Open Opt. J. **7**(1), 104–127 (2013).
2. X. Bao and L. Chen, "Recent Progress in Distributed Fiber Optic Sensors," Sensors **12**(7), 8601–8639 (2012).
3. M. Froggatt and J. Moore, "High-spatial-resolution distributed strain measurement in optical fiber with Rayleigh scatter," Appl. Opt. **37**(10), 1735 (1998).
4. Z. Ding, C. Wang, K. Liu, J. Jiang, D. Yang, G. Pan, Z. Pu, and T. Liu, "Distributed Optical Fiber Sensors Based on Optical Frequency Domain Reflectometry: A review," Sensors **18**(4), 1072 (2018).
5. S. Kreger, D. Gifford, M. Froggatt, B. Soller, and M. Wolfe, "High Resolution Distributed Strain or Temperature Measurements in Single- and Multi-Mode Fiber Using Swept-Wavelength Interferometry," in *Optical Fiber Sensors, OSA Technical Digest (CD)* (Optical Society of America, 2006), paper ThE42.
6. M. Xu, L. Reekie, J. Dakin, and J. Archambault, "Discrimination between strain and temperature effects using dual-wavelength fibre grating sensors," Electron. Lett. **30**(13), 1085–1087 (1994).
7. M. Emmanuel and Y. Ouerdane, "Dual-Fibre Bragg Grating Sensor for Simultaneous Temperature and Strain Sensing of Composite Materials Manufacturing," in *proceeding of EWSHM - 7th European Workshop on Structural Health Monitoring*, L. Cam, ed. (Academic, Nantes, France, 2014), pp. 946–953.
8. S. Mondal, U. Tiwari, G. Poddar, V. Mishra, N. Singh, S. Jain, S. Sarkar, K. Chattoypadhya, and P. Kapur, "Single fiber Bragg grating sensor with two sections of different diameters for longitudinal strain and temperature discrimination with enhanced strain sensitivity," Rev. Sci. Instrum. **80**(10), 103106 (2009).
9. S. Oh, W. Han, U. Paek, and Y. Chung, "Discrimination of temperature and strain with a single FBG based on the birefringence effect," Opt. Express **12**(4), 724 (2004).
10. X. Lu, MA. Soto, and L. Thévenaz, "Discrimination of temperature and strain by combined refractive index and birefringence measurements using coherent Rayleigh sensing," in *proceeding of IEEE Conference on Optical Fiber* (Institute of Electrical and Electronics Engineers, Jeju Island, 2017), pp. 1–4.
11. W. Li, L. Chen, and X. Bao, "Compensation of temperature and strain coefficients due to local birefringence using optical frequency domain reflectometry," Opt. Commun. **311**, 26–32 (2013).
12. K. Kinzo, Y. Yamauchi, and A. Guzik, "Study of optical fibers strain-temperature sensitivities using hybrid Brillouin-Rayleigh System," Photonic Sens. **4**(11), 1–11 (2014).
13. D. Zhou, W. Li, L. Chen, and X. Bao, "Distributed Temperature and Strain Discrimination with Stimulated Brillouin Scattering and Rayleigh Backscatter in an Optical Fiber," Sensors **13**(2), 1836–1845 (2013).
14. Z. Ding, D. Yang, Y. Du, K. Liu, Y. Zhou, R. Zhang, Z. Xu, J. Jiang, and T. Liu, "Distributed strain and temperature discrimination using two types of fiber in OFDR," IEEE Photonics J. **8**(5), 1–8 (2016).
15. D. Yang, T. Liu, Z. Ding, Q. Han, K. Liu, J. Jiang, Q. Chen, and B. Feng, "Cryogenic temperature measurement using Rayleigh backscattering spectra shift by OFDR," IEEE Photonics Technol. Lett. **26**(11), 1150–1153 (2014).
16. A. Wosniok, D. Skoczowsky, M. Schukar, S. Pötzsch, S. Pötschke, and S. Krüger, "Fiber optic sensors for high-temperature measurements on composite tanks in fire," J. Civ. Struct. Health Monit. **9**(3), 361–368 (2019).
17. A. Faustov, A. Gussarov, M. Wuilpart, A. A. Fotiadi, L. B. Liokumovich, O. I. Kotov, I. O. Zolotovskiy, A. L. Tomashuk, T. Deschoutheete, and P. Mégret, "Distributed optical fibre temperature measurements in a low dose rate radiation environment based on Rayleigh backscattering," Proc. SPIE **8439**, 84390C (2012).
18. S. Pavol, K. Hicke, and K. Krebber, "Distributed Fiberoptic Sensor for Simultaneous Humidity and Temperature Monitoring Based on Polyimide-Coated Optical Fibers," Sensors **19**(23), 5279 (2019).
19. S. Wang, K. Lasn, C. Elverum, D. Wan, and A. Echtermeyer, "Novel in-situ residual strain measurements in additive manufacturing specimens by using the Optical Backscatter Reflectometry," Addit. Manuf. **32**, 101040 (2020).
20. P. A. Kisaka, E. M. Beres-Pawlik, J. Wojcik, and W. Wojcik, "Fiber Bragg grating sensors for temperature measurement," Proc. SPIE **5576**, 270–276 (2004).
21. R. Rajinikumar, K. G. Narayankhedkar, G. Krieg, M. Suber, A. Nyilas, and K. P. Weiss, "Fiber Bragg gratings for sensing temperature and stress in super conducting coils," IEEE Trans. Appl. Supercond. **16**(2), 1737–1740 (2006).

Optics EXPRESS

22. J. Komma, C. Schwarz, G. Hofmann, D. Heinert, and R. Nawrodt, "Thermo-optic coefficient of silicon at 1550 nm and cryogenic temperatures," Appl. Phys. Lett. **101**(4), 041905 (2012).
23. W. Wang, Y. Yu, Y. Geng, and X. Li, "Measurements of thermo-optic coefficient of standard single mode fiber in large temperature range," In *proceeding of Optical Instruments and Technology: Optical Sensors and Applications*, (Academic, Beijing, 2015), pp. 96200.
24. F. Della Corte, M. Esposito Montefusco, L. Moretti, I. Rendina, and G. Cocorullo, "Temperature dependence analysis of the thermo-optic effect in silicon by single and double oscillator models," J. Appl. Phys. **88**(12), 7115–7119 (2000).
25. G. Gosh, "Sellmeier coefficients and dispersion of thermo-optic coefficients for some optical glasses," Appl. Opt. **36**(7), 1540–1546 (1997).
26. G. Ghosh, "Model for the thermo-optic coefficients of some standard optical glasses," J. Non-Cryst. Solids **189**(1-2), 191–196 (1995).
27. K. Lasn, E. Sæter, and A. Echtermeyer, "Sensing of Structural Damage with OBR Based Fibre-Optic Networks," (STO-Meeting Proceedings Paper, 2018), https://ntnuopen.ntnu.no/ntnu-xmlui/handle/11250/2587611.
28. H. M. Lund, "Health monitoring of composites using optical fibres," (Master's thesis, NTNU, 2012), https://ntnuopen.ntnu.no/ntnu-xmlui/handle/11250/241661.